AMERICAN SOCIETY FOR MICROBIOLOGY | Journal of Virology®

GENOME REPLICATION AND REGULATION OF VIRAL GENE EXPRESSION

Shiftless Restricts Viral Gene Expression and Influences RNA Granule Formation during Kaposi's Sarcoma-Associated Herpesvirus Lytic Replication

William Rodriguez,[a] Timothy Mehrmann,[a] David Hatfield,[a] Mandy Muller[a]

[a]Department of Microbiology, University of Massachusetts, Amherst, Massachusetts, USA

ABSTRACT Herpesviral infection reflects thousands of years of coevolution and the constant struggle between virus and host for control of cellular gene expression. During Kaposi's sarcoma-associated herpesvirus (KSHV) lytic replication, the virus rapidly seizes control of host gene expression machinery by triggering a massive RNA decay event via a virally encoded endoribonuclease, SOX. This virus takeover strategy decimates close to 80% of cellular transcripts, reallocating host resources toward viral replication. The host cell, however, is not entirely passive in this assault on RNA stability. A small pool of host transcripts that actively evade SOX cleavage has been identified over the years. One such "escapee," C19ORF66 (herein referred to as Shiftless [SHFL]), encodes a potent antiviral protein capable of restricting the replication of multiple DNA and RNA viruses and retroviruses, including KSHV. Here, we show that SHFL restricts KSHV replication by targeting the expression of critical viral early genes, including the master transactivator protein, KSHV ORF50, and thus subsequently the entire lytic gene cascade. Consistent with previous reports, we found that the SHFL interactome throughout KSHV infection is dominated by RNA-binding proteins that influence both translation and protein stability, including the viral protein ORF57, a crucial regulator of viral RNA fate. We next show that SHFL affects cytoplasmic RNA granule formation, triggering the disassembly of processing bodies. Taken together, our findings provide insights into the complex relationship between RNA stability, RNA granule formation, and the antiviral response to KSHV infection.

IMPORTANCE In the past 5 years, SHFL has emerged as a novel and integral piece of the innate immune response to viral infection. SHFL has been reported to restrict the replication of multiple viruses, including several flaviviruses and the retrovirus HIV-1. However, to date, the mechanism(s) by which SHFL restricts DNA virus infection remains largely unknown. We have previously shown that following its escape from KSHV-induced RNA decay, SHFL acts as a potent antiviral factor, restricting nearly every stage of KSHV lytic replication. In this study, we set out to determine the mechanism by which SHFL restricts KSHV infection. We demonstrate that SHFL impacts all classes of KSHV genes and found that SHFL restricts the expression of several key early genes, including KSHV ORF50 and ORF57. We then mapped the interactome of SHFL during KSHV infection and found several host and viral RNA-binding proteins that all play crucial roles in regulating RNA stability and translation. Lastly, we found that SHFL expression influences RNA granule formation both outside and within the context of KSHV infection, highlighting its broader impact on global gene expression. Collectively, our findings highlight a novel relationship between a critical piece of the antiviral response to KSHV infection and the regulation of RNA-protein dynamics.

KEYWORDS KSHV, ORF50, RNA decay, SHFL

Kaposi's sarcoma-associated herpesvirus, or human herpesvirus 8 (KSHV/HHV-8), is an oncogenic gamma 2 herpesvirus and the causative agent of multiple malignancies, including its namesake, Kaposi's sarcoma (KS), and two lymphoproliferative disorders:

Editor Jae U. Jung, Lerner Research Institute, Cleveland Clinic

Address correspondence to Mandy Muller, mandymuller@umass.edu.

The authors declare no conflict of interest.

Received 21 September 2022
Accepted 12 October 2022
Published 3 November 2022

primary effusion lymphoma (PEL) and multicentric Castleman's disease (MCD) (1, 2). Like all herpesviruses, KSHV infection is defined by two distinct phases: a lifelong viral latency, where most of viral gene expression is suppressed, broken only by active lytic viral replication (3). KSHV latency establishment facilitates virus persistence within its human host for decades, reflecting KSHV's exceptional capacity to evade detection by host immune surveillance. Sporadically, in response to a growing list of environment and intracellular triggers, KSHV switches into a lytic replicative state, swiftly remodeling and repurposing the host cell toward viral gene expression and progeny virion assembly (3, 4). Normally, the human immune response keeps this life cycle in check by actively suppressing KSHV infection. However, in immunocompromised individuals such as untreated AIDS patients, KSHV infection can lead to the production of protumorigenic factors (both viral and host) that drive forward KSHV-associated malignancies (5, 6).

Successful KSHV lytic replication relies on the ability of the virus to rapidly seize and maintain control of cellular gene expression following reactivation from latency. One KSHV stratagem for taking over these resources is to trigger a global RNA decay event termed host shutoff, which is orchestrated by KSHV ORF37 (SOX), a virally encoded endoribonuclease (7–10). SOX expression decimates most of the host transcriptome, releasing host resources, once bound to cellular mRNA and now free for coordination of viral gene expression (10–12).

While the breadth of mRNA targeted by SOX and other viral host shutoff proteins is expansive, we and others have found that a select few host mRNAs are spared from degradation (13, 14). These transcripts, termed escapees, are spared from a range of viral—but not host—endonucleases (13–18) and appear to actively escape cleavage via a protective RNA element located within their 3′ untranslated regions (UTRs) that we refer to as the SOX-resistant element (SRE). These "dominant" escapees previously included only the host interleukin-6 (IL-6) (16) and the growth arrest and DNA damage-inducible 45 beta (GADD45B) (15). More recently, we identified yet another SRE-bearing mRNA, C19ORF66 (RyDEN, IRAV, SVA-1, Shiftless), herein referred to as SHFL, a cellular transcript that evades cleavage by not only SOX but also multiple herpesviral endonucleases and even the influenza A virus (IAV) PA-X endonuclease (18). Upon further investigation, we demonstrated that SHFL is a stringent anti-KSHV factor, restricting KSHV lytic reactivation from latency and all subsequent stages of lytic viral replication.

SHFL is an interferon-stimulated gene (ISG) that is demonstrably a vital piece of the innate immune response to viral infection, capable of suppressing the replication of multiple DNA and RNA viruses and retroviruses (18–27). Studies of SHFL function over the past 5 years have revealed its multifaceted capacity to negatively modulate viral RNA stability, viral gene translation, and even viral protein stability through interactions with cellular cofactors that coordinate these processes, such as cytoplasmic polyadenylate binding protein 1 (PABPC1), La ribonucleoprotein domain family member 1 (LARP1), and the RNA helicase MOV10 (19, 20). SHFL can also induce the degradation of viral proteins through a variety of pathways, including lysosomal degradation (22) and ubiquitination via the E3 ubiquitin ligase MARCH8 (25). SHFL is also among the first human genes identified as capable of restricting the -1 programmed ribosomal frameshift (-1PRF) of both HIV-1 and the current pandemic-associated virus, severe acute respiratory syndrome coronavirus 2 (SARS-CoV-2) (21, 24). SHFL thus has emerged as a critical piece of the innate host defense array of ISGs against viral infection.

The SHFL protein is 291 amino acids (aa) long, consisting of several computationally predicted structures including eight α-helices, seven β-strands, a zinc ribbon motif (aa 112 to 135), a coiled-coil motif (aa 261 to 285), a nuclear localization signal (NLS; aa 121 to 173), a nuclear export signal (NES; aa 261 to 269), and, lastly, a glutamic acid (E)-rich motif in the C terminus. Interestingly, SHFL contains two functionally distinct domains. The first, identified by Suzuki et al. in 2016, contains the zinc ribbon motif and the functional nuclear localization signal, which spans aa 102 to 150 (19). This domain was shown to be required for SHFL-mediated restriction of dengue virus (DENV) replication and for the binding of SHFL to DENV genomic RNA. More recently, it was shown

that three arginine residues within this domain (R131, R133, and R136) are important for the capacity of SHFL to bind viral RNA *in vitro* (28). The second domain, identified by Wang et al. in 2019, spanning aa 164 to 199, was shown to be important for SHFL-mediated restriction of the −1PRF of human and viral genes, and it is required to restrict the replication of both HIV-1 and Japanese encephalitis virus (JEV) (21, 26). SHFL complex and versatile structures and domains thus appear to mirror its diversity of functions (29).

While the breadth of SHFL activity continues to be unraveled, the molecular mechanism(s) behind SHFL's function, especially during DNA virus infection, remains largely unknown. Here, we demonstrate that SHFL broadly restricts KSHV lytic gene expression, including that of the master latent-to-lytic switch protein, KSHV's ORF50 (RTA), an impact that catastrophically dysregulates the initiation of the KSHV lytic gene cascade. Upon further investigation, we found that the SHFL interactome is dominated by RNA-binding proteins (RBPs) during both KSHV latency and lytic replication. Surprisingly, we found that SHFL negatively influences the assembly of a key RNP granule type, RNA processing bodies (P-bodies), while simultaneously inducing the formation of stress granules (SGs) both outside and within the context of KSHV infection. Lastly, SHFL also interacts with and restricts the expression of the KSHV RNA-binding protein ORF57, a broad regulator of viral RNA fate. Taken together, our findings highlight that SHFL is an integral piece of the virus-host arms race between KSHV and its human host for control of cellular gene expression during lytic replication following its escape from SOX cleavage.

RESULTS

SHFL broadly restricts KSHV lytic gene expression. SHFL is a potent antiviral factor capable of restricting the replication of multiple viral families, including flaviviruses, alphaviruses, and retroviruses. Consistently, we have previously demonstrated that SHFL also restricts KSHV lytic replication (18). To determine the mechanism underlying this restriction, we first investigated the breadth of SHFL impact on KSHV lytic gene expression. First, we examined an array of viral genes spanning all kinetic classes, at both the RNA and protein levels, when overexpressing SHFL in the KSHV-positive renal carcinoma cell line iSLK.Bac16 (herein referred to as iSLK.WT). We observed that SHFL moderately to severely restricted gene expression for all lytic viral gene products tested (Fig. 1A and B). Given this extensive effect on lytic gene expression, we hypothesized that instead of individually targeting each of these genes, SHFL could target one of the earliest and most critical regulators of the viral lytic gene cascade: KSHV's ORF50. ORF50 (RTA) is a master viral transcriptional regulator that controls the switch between KSHV latency and active lytic replication (30–34). ORF50 alone has been shown to be both necessary and sufficient for lytic reactivation and the transactivation of multiple lytic gene promoters, including its own (31). In line with our hypothesis, using both overexpression and knockdown approaches, we confirmed that ORF50 expression is severely restricted by SHFL (Fig. 1C and D). Furthermore, in iSLK.WT cells, ORF50 is expressed from two distinct promoters: from the "endogenous" one on the viral genome (viral ORF50 [vORF50]) and from an exogenous doxycycline-inducible promoter used to artificially promote the latent-to-lytic switch (35). The ORF50 detected in our initial reverse transcription-quantitative PCR (RT-qPCR) screen represents the total amount of ORF50 (total ORF50) expressed upon induction of lytic reactivation from both promoters. During lytic replication, once initially expressed from the doxycycline promoter, ORF50 will transactivate its own promoter on the viral genome (vORF50), potentiating a positive-feedback loop (36). To determine whether the effect of SHFL on total ORF50 mRNA levels was due to loss of transcription from the native viral promoter, we next designed a set of primers to differentially assess vORF50 versus total ORF50 expression (Fig. 1E). We observed that SHFL was able to repress vORF50 mRNA levels derived from the viral genome promoter, suggesting that SHFL expression interferes with the ORF50 positive-feedback loop possibly through either a direct influence on ORF50 transactivation or a posttranscriptional inhibition of ORF50. We next performed a

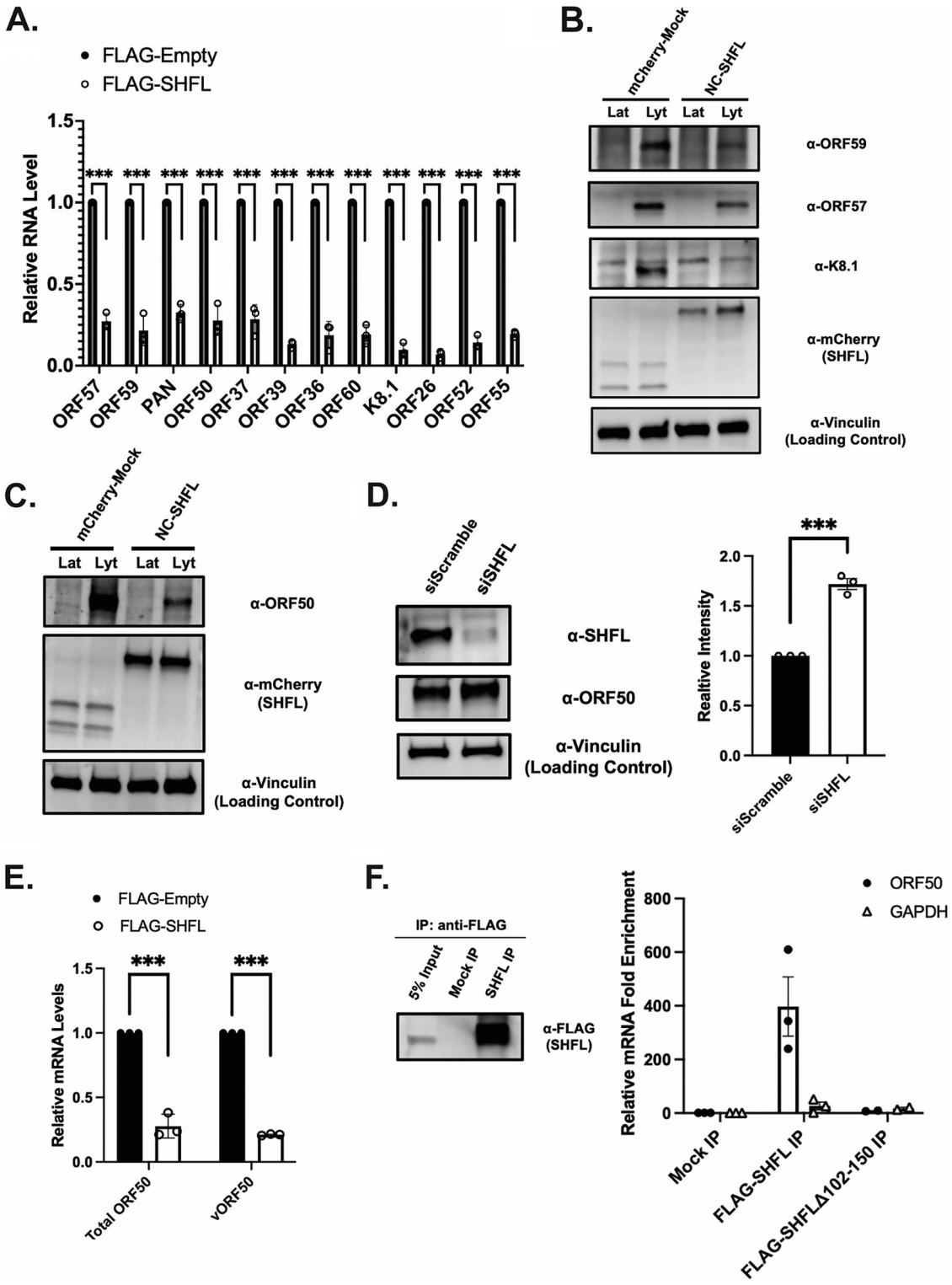

FIG 1 SHFL broadly restricts KSHV lytic gene expression. (A) KSHV-positive iSLK.WT cells were transfected with a FLAG-tagged SHFL or a FLAG-empty vector and reactivated with doxycycline and sodium butyrate for 48 h. Total RNA was then harvested and subjected to RT-qPCR to measure mRNA levels of the indicated viral early, delayed early, and late genes. (B and C) iSLK.WT cells were first transfected with either an N-terminally tagged mCherry-SHFL (NC-SHFL) or an mCherry-empty vector. Cells were then reactivated for 48h (Lyt) or left untreated (Lat). Cells were then harvested, lysed, resolved by SDS-PAGE, and immunoblotted with the indicated antibodies. (D) Unreactivated or reactivated iSLK.WT cells were treated with either siRNA targeting SHFL or control scramble siRNAs for 48 h. siRNA-treated cells were then harvested, lysed, resolved by SDS-PAGE, and immunoblotted with the indicated antibodies. (E) iSLK.WT cells were transfected with either a FLAG-empty or FLAG-SHFL vector and reactivated for 48 h. Total RNA was then harvested and subjected to RT-qPCR using primers targeting the viral genome-derived ORF50 (vORF50). (F) HEK293T cells were first transfected

(Continued on next page)

4-thiouridine (4sU) assay to directly measure nascent total and vORF50 RNA transcription in SHFL-transfected iSLK.WT cells to assess whether SHFL directly impacted ORF50 transcription rates. We found that vORF50 transcription was not significantly affected by SHFL (see Fig. S1 in the supplemental material) at 48 h after reactivation from latency. Lastly, given the significant reduction of ORF50 protein and RNA levels upon SHFL expression and SHFL's known RNA binding capacity, we next hypothesized that SHFL could bind to ORF50 mRNA to mediate a posttranscriptional mechanism of restriction. We thus next checked whether SHFL could bind to ORF50 mRNA using RNA immunoprecipitation (RIP). HEK293T cells were transfected with both FLAG-SHFL and a C-terminal strep-tagged ORF50, SHFL was pulled down using M2 FLAG beads and ORF50 RNA was detected by RT-qPCR (Fig. 1F). Given these findings, we hypothesized that SHFL-mediated repression of ORF50 could stem from a destabilization of ORF50 mRNA. However, using an actinomycin D assay, we did not observe any significant difference in ORF50 mRNA half-life ($t_{1/2}$; 4 h) upon SHFL expression (Fig. S2). Collectively, these data suggest that SHFL restricts lytic gene expression posttranscriptionally and in a manner independent from viral RNA stability.

Several previous studies of SHFL have identified two functional domains required for its ability to both restrict viral infection and bind target mRNAs (19, 21, 23, 26). One of these domains, amino acids (aa) 102 to 150, has been shown to be critical to maintain its interaction with RNA-binding proteins (16), and three specific residues within this domain (R131, R133, and R136) have been reported to mediate the ability of SHFL to bind to viral RNA *in vitro* (28). Given these previous studies, we next sought to determine if this domain of SHFL is also required to modulate ORF50 expression and to maintain its interaction with ORF50 mRNA. To test this, we first designed an SHFL mutant with a deletion of this putative RNA binding domain (aa 102 to 150), herein referred to as SHFLΔ102-150. HEK293T cells were transfected with either a FLAG-empty vector or FLAG-SHFLΔ102-150 and lytic reactivation was induced for 48 h using doxycycline and sodium butyrate. We found that the SHFLΔ102-150 mutant failed to bind ORF50 mRNA (Fig. 1F). Taken together, our results show that SHFL specifically binds to ORF50 mRNA, restricts ORF50 expression, and therein restrict KSHV lytic replication.

SHFL interacts with RNA-binding proteins during KSHV infection. To better understand how SHFL regulates ORF50 expression, we next set out to map its interaction network throughout KSHV infection. iSLK.WT cells were either left latent or reactivated for 48 h with doxycycline and sodium butyrate to trigger the KSHV lytic cycle. After verifying SHFL pulldown efficiency (Fig. S3), the SHFL interactome during KSHV infection was mapped using liquid chromatography-tandem mass spectrometry (LC-MS/MS). In total, 98 unique proteins were identified as SHFL interactors, of which 9 were exclusively detected in the latent cells and 12 were exclusively found in lytic cells (Fig. 2A and Table S1). The remaining interactors span both latency and lytic replication and include the known SHFL interactor PABPC1, which we also confirmed via coimmunoprecipitation (Fig. S3) (19). Gene Ontology (GO) analysis on SHFL interactors revealed several functional categories, including RNA binding and ubiquitin ligase binding, confirming previously suspected roles for SHFL in both RNA and protein stability (Fig. 2B and C and Table S2). Notably, several important cellular RNA binding proteins were identified that are known constituents of cytoplasmic stress granules, including PABPC1, KPNA2, DDX3X, FUS, and HNRNPK (37–40). Intriguingly, we also detected three viral proteins as potential SHFL interactors: ORF59, the KSHV DNA processivity factor; ORF57, the master regulator of KSHV RNA fate; and ORF52, a tegument protein that inhibits cytosolic viral DNA sensing via cGAS/STING (41–43).

FIG 1 Legend (Continued)
with either a FLAG-empty, FLAG-SHFL, or FLAG-SHFLΔ102-150 vector. Cells were then harvested and lysed, and RNA immunoprecipitation (RIP) was performed using M2 FLAG beads or control beads (mock IP). Following reverse cross-linking, total RNA was harvested and subjected to RT-qPCR using primers as indicated. Statistics were determined using Student's paired *t* test between control and experimental groups; error bars represent standard errors of the means ($n = 3$ independent biological replicates). **, $P < 0.01$; ***, $P < 0.001$.

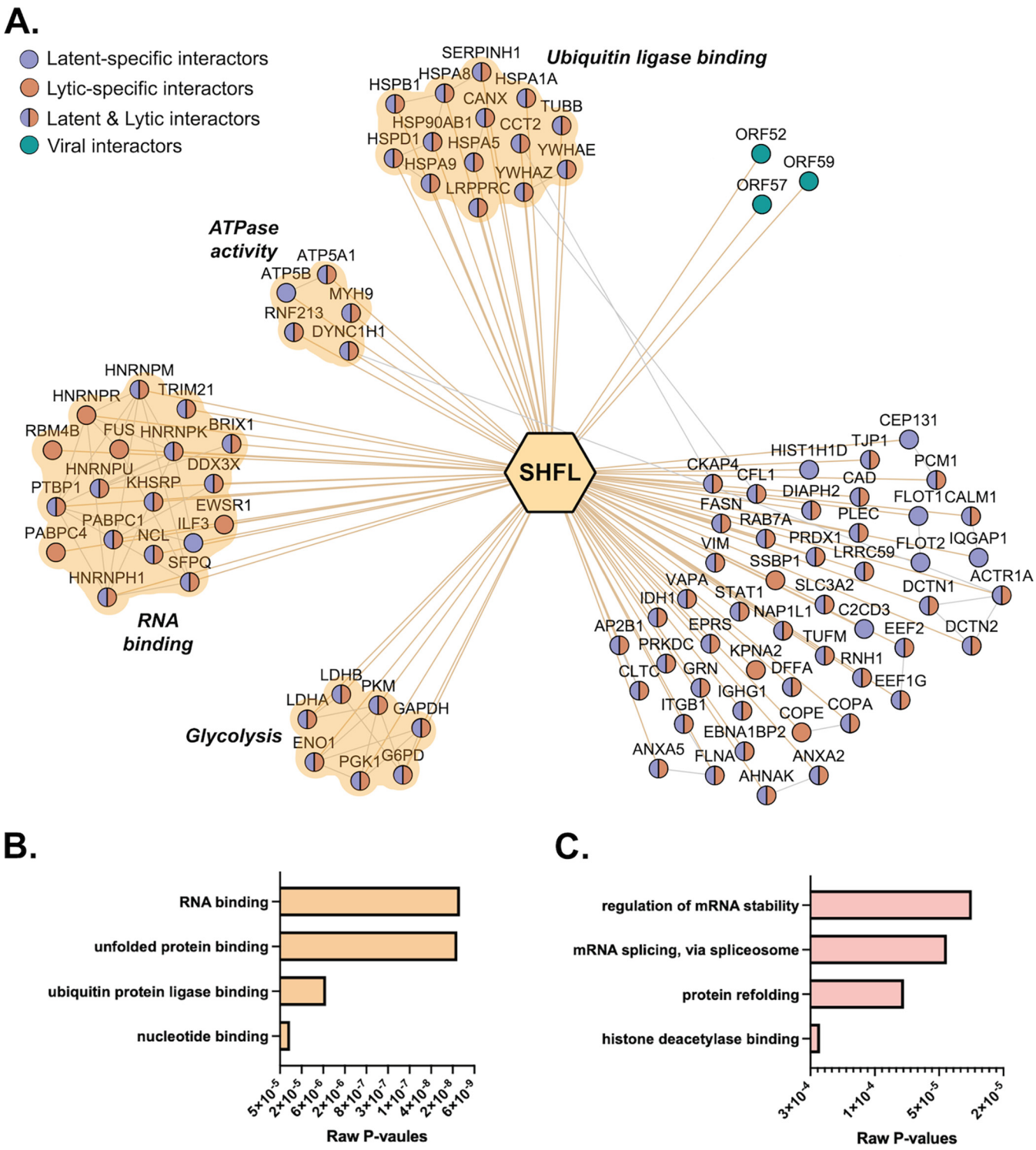

FIG 2 Determination of SHFL interactome during KSHV infection. (A) iSLK.WT cells were reactivated for 72 h and subjected to mass spectrometry. Network generated by Cytoscape represents the interactome of SHFL during both KSHV latency and lytic replication. A total of 92 high-confidence interactions between SHFL (center hexagon) and human proteins (nodes) were identified by mass spectrometry, along with 3 viral proteins (blue nodes). Interactions exclusively identified in latent samples are labeled in purple, while those identified specifically in the lytic samples are identified in orange. Physical interactions among host proteins (thin gray lines) were manually curated from the STRING and IntAct databases. Gene Ontology (GO) enrichment analysis was performed on the human interacting proteins of SHFL using the DAVID bioinformatic database. Top enriched clusters are identified on the network. Bar graphs represent the raw *P* values for the most enriched GO terms by molecular function (B) and biological process (C).

SHFL influences P-body and SG dynamics during KSHV infection. Cytoplasmic RNA granules, such as stress granules (SGs) and processing bodies (P-bodies), are membrane-free, phase-separated ribonucleoprotein (RNP) complexes that function in the storage, translational arrest, and/or degradation of RNA in the cytoplasm (44–51). Given the enrichment of SG components in our mass spectrometry data, we next set out to determine whether SHFL localizes to RNP granules. First, HEK293T cells were transfected with either a mock vector or an SHFL-expressing vector. Cells were then fixed, permeabilized, and immunostained for known RNP granule markers, including DEAD-box helicase 6 (DDX6) and enhancer of mRNA decapping 4 (EDC4) for P-bodies and G3BP stress granule assembly factor 1 (G3BP1) and cytotoxic granule associated RNA-binding protein (TIA-1) for stress granules. RNP granule quantification was performed using CellProfiler to analyze immunofluorescence images stained for the hallmark P-body and SG resident proteins as described in Materials and Methods. In HEK293T cells, SHFL remained diffusely cytoplasmic as we observed previously (16) (Fig. 3A). However, surprisingly, we observed that SHFL expression drastically restricted the number of DDX6 (Fig. 3A) and EDC4 (Fig. 3B) puncta per cell relative to mock transfection. Furthermore, we also observed that there was a simultaneous induction of "SG-like densities" localizing with SHFL in these SHFL-expressing cells (Fig. 3B). A similar effect was found with TIA-1, a second SG marker, in SHFL-expressing cells (Fig. S4).

To determine whether SHFL expression also influences P-body numbers during KSHV infection, we next transfected iSLK.WT cells with SHFL, left them latent or reactivated them with doxycycline and sodium butyrate, and stained them for the same RNP granule markers. As reported in previous literature, we observed no impact on P-body formation in untransfected KSHV latent cells and a corresponding decrease in P-body numbers upon lytic reactivation from latency (Fig. S5) (52). In line with our observations in HEK293T cells, SHFL expression in both KSHV latent and reactivated cells appears to restrict the number of P-body foci (Fig. 3C). Interestingly, we did not observe a corresponding decrease in DDX6 protein expression in SHFL-expressing iSLK.WT cells (Fig. S6), suggesting that SHFL expression may impact the expression of other P-body scaffolding factors or trigger their relocalization. In summary, our data suggest that SHFL may have more global influence over cellular gene expression, including perhaps both host and viral genes. The induction of stress granule-like densities by SHFL also points toward an impact on global gene translation.

SHFL interacts with and restricts the expression of KSHV ORF57. Given SHFL effect on ORF50 expression and its influence over RNP granule dynamics, we were particularly intrigued by its interaction with KSHV ORF57 detected in our mass spectrometry screen. We first confirmed the interaction between SHFL and ORF57 by immunoprecipitation and reverse immunoprecipitation (Fig. 4A). While SHFL overexpression in iSLK.WT cells resulted in lower expression of ORF57 mRNA (Fig. 1A), transient coexpression of SHFL and ORF57 in HEK293T cells seemed to have no effect on ORF57 mRNA (Fig. 4D), reinforcing the idea that the effect observed on viral mRNA levels in KSHV-positive cells was posttranscriptional and stemmed from an ORF50-dependent mechanism. We thus hypothesized that SHFL could influence the expression of ORF57, which, in turn, could be a mechanistic underpin to SHFL-mediated translational repression of ORF50. First, we showed that the interaction between ORF57 and SHFL was drastically reduced when the samples were treated with RNase, suggesting that SHFL and ORF57 may be brought together in a complex around viral and perhaps even host RNAs (Fig. 4A). Next, we found that SHFL coexpression with ORF57 markedly reduced the amount of ORF57 protein, but not mRNA levels, expressed in HEK293T cells (Fig. 4B to D), pointing once again to a mechanism beyond viral gene transcription and RNA stability. Next, given the critical nature of the aa 102 to 150 binding domain for, the binding of SHFL to viral mRNA we next hypothesized that this domain could also affect the interaction between SHFL and ORF57. In accordance with this, using coexpression of FLAG-SHFLΔ102-150 and ORF57-6× HIS followed by coimmunoprecipitation of ORF57, we found that ORF57 did not interact with this SHFL mutant (Fig. 4B). Given that SHFL and ORF57 appear to target

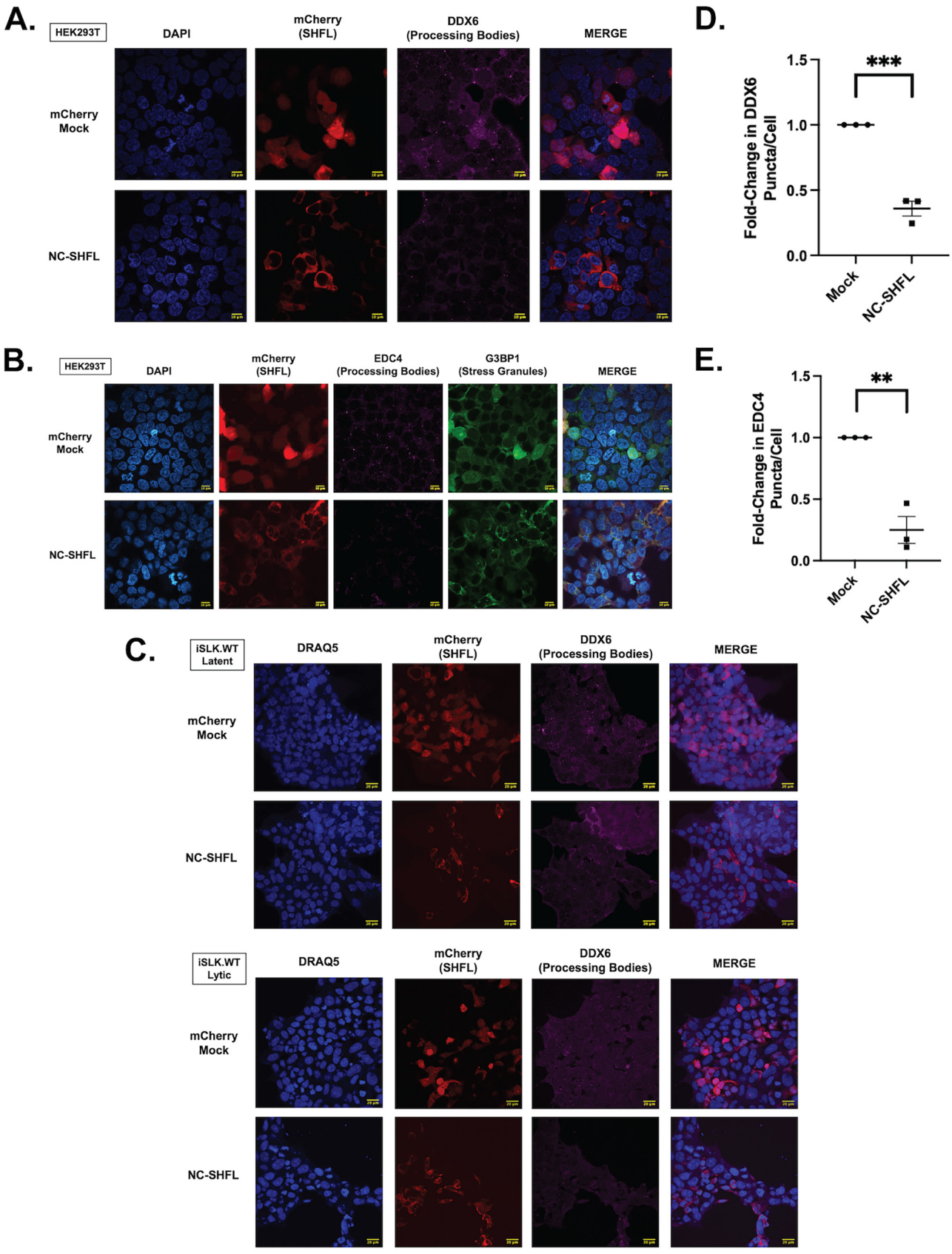

FIG 3 SHFL expression influences RNA granule formation. (A and B) HEK293T cells were transfected with either NC-SHFL or an mCherry-only (mock) vector. Cells were subjected to immunofluorescence assay and stained for the indicated processing body (DDX6 or EDC4 [purple]) or stress granule

(Continued on next page)

several of the same proteins, it is likely that they form a large ribonucleoprotein complex. Interestingly, probing immunoprecipitated from cells coexpressing SHFL and ORF57, we found interactions between SHFL, polyadenylate-binding cytoplasmic protein 1 (PABPC1), and DDX3X but weak interactions with KPNA2 and FUS (Fig. 4C). Lastly, we wondered whether SHFL and ORF57 colocalize, and if so, whether this colocalization coincides with SHFL-induced SGs as shown in Fig. 3. To test this, we again cotransfected SHFL alongside ORF57 in HEK293T cells and performed an immunofluorescence assay. Cells were then fixed, permeabilized, and immunostained for both ORF57 and the SG marker TIA-1. Interestingly, while ORF57 was predominately nuclear, distinct cytoplasmic densities of SHFL appeared to localize alongside densities of ORF57 and TIA-1 in the cytoplasm (Fig. 4E and F). We also did not see the same level of SG marker accumulation with TIA-1 as previously observed with expression of SHFL alone, indicating that ORF57 may still have been dispersing SHFL-induced SGs. While TIA-1 is an SG marker, the protein itself serves a primary function in orchestrating translational arrest (53, 54). Therefore, these data indicate that SHFL may restrict the translation of ORF57 and thereby its expression.

DISCUSSION

Since its initial characterization by Suzuki et al. in 2016, C19ORF66 (here referred to as SHFL) has emerged as a critical piece of the innate immune response to viral infection. SHFL restricts the replication of a vast assortment of DNA and RNA viruses and retroviruses to various degrees and is itself an interferon-stimulated gene (ISG) (20, 27). Fascinatingly, for each virus that SHFL restricts, a different mechanism has been described. These inhibition strategies range dramatically from the targeting of viral RNA and protein stability to restriction of viral protein translation and even the architecture of viral replication organelles (23). SHFL is also the first human gene found to actively restrict the −1 programmed ribosomal frameshift (−1PRF), a translation strategy conserved across several eukaryotic viruses, mammals, and even prokaryotes (19, 22, 55–57). Collectively, these studies reflect the versatility of SHFL to broadly influence gene expression and therein directly impact the balance between host and viral gene expression during infection. Similarly, we have previously identified SHFL as a transcript that actively escapes virus-induced RNA decay during KSHV infection (18). Furthermore, we also found that the SHFL protein is a potent anti-KSHV factor, restricting nearly every stage of KSHV lytic replication following reactivation from latency. Here, we present our recent efforts toward understanding the mechanism(s) by which SHFL restricts KSHV infection.

Looking broadly at KSHV lytic gene expression, we found that transient SHFL expression stringently restricts all classes of lytic genes at both the RNA and protein levels. Taken together with our previous observations of SHFL knockdown (18), this restriction is likely a domino effect from a direct impact of SHFL on KSHV early gene expression. In line with this, we observed a significant restriction of KSHV ORF50 (RTA), which encodes the master latent-to-lytic switch protein responsible for the initiation of the entire lytic gene cascade (31). Upon further investigation, we found that SHFL binds to ORF50 mRNA but does not significantly impact the half-life of ORF50 mRNA during lytic replication. Given the significant decrease in ORF50 mRNA levels in the absence of RNA decay, we next investigated the transcription of the viral genome-derived ORF50, whose expression is controlled by a positive-feedback loop initiated by the activation of the doxycycline-inducible ORF50 in the iSLK.WT cell model. We found that vORF50 mRNA levels were significantly impacted upon SHFL overexpression, but surprisingly, its transcription rate was unaffected. This would suggest that SHFL-mediated

FIG 3 Legend (Continued)
markers (G3BP [green]). (C) iSLK.WT cells were transfected with either an NC-SHFL or mCherry-only (mock) vector and left latent or reactivated for 48 h. Cells were then subjected to immunofluorescence assay and stained with the indicated antibodies. (D and E) The number of P-body puncta per cell was quantified using the CellProfiler pipeline as described in Materials and Methods and normalized to the mock control within each replicate. Scale bar represents 10 μm. Statistics were determined using Student's paired *t* test between control and experimental groups; error bars represent standard errors of the means ($n = 3$ independent biological replicates). **, $P < 0.01$; ***, $P < 0.001$.

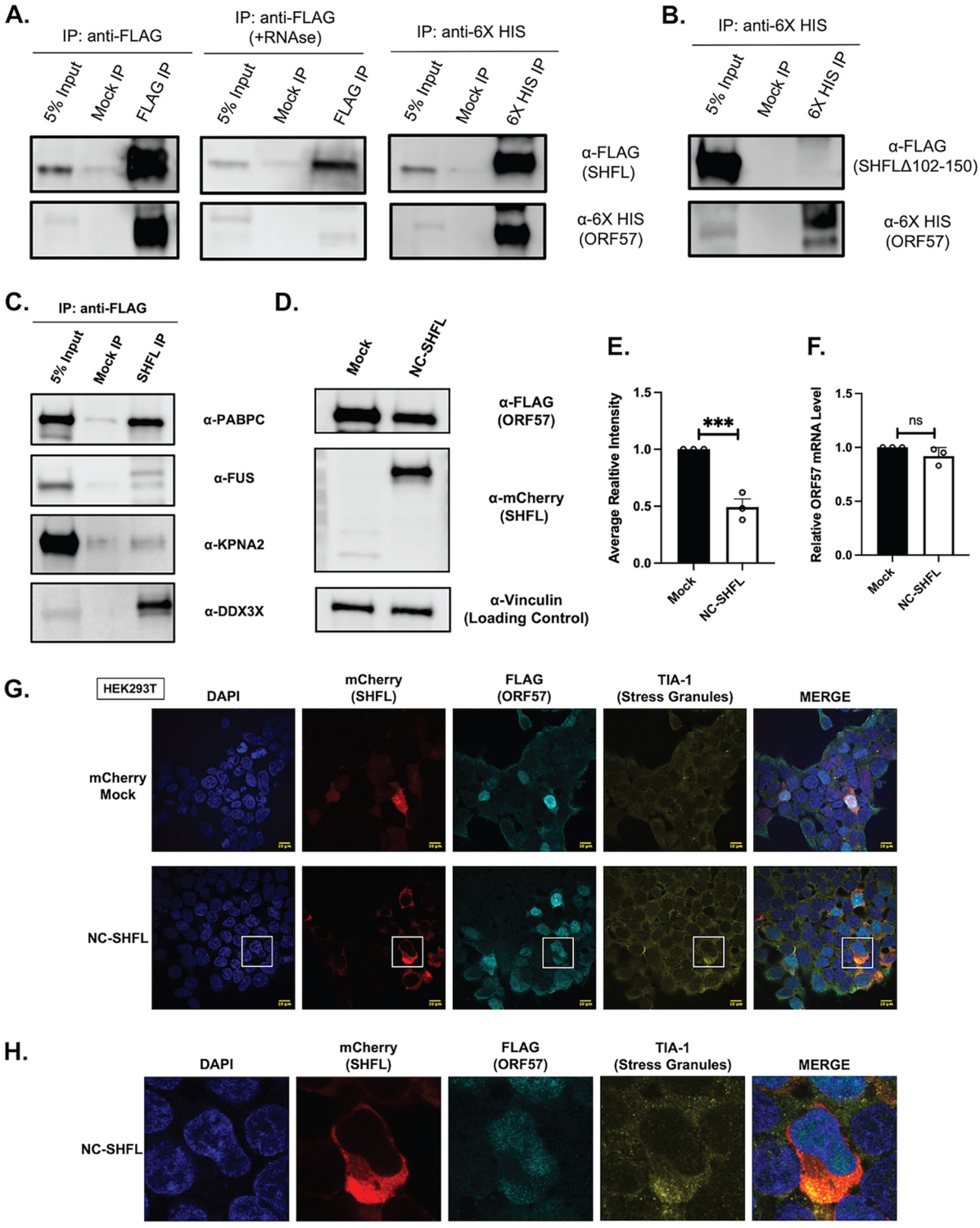

FIG 4 SHFL interacts with and restricts the expression of KSHV ORF57. (A and B) HEK293T cells were cotransfected with either FLAG-SHFL or FLAG-SHFLΔ102-150 and a 6×HIS-tagged ORF57. Cells were then harvested and lysed, and co-IP was performed using FLAG-tag affinity beads. Reverse co-IP was performed using anti-6×HIS antibody. RNase co-IP was performed similarly to FLAG co-IP with an additional RNase A and RNase T1 treatment prior to overnight co-IP. (C) HEK293T cells were transfected with both FLAG-SHFL and ORF57-6×HIS. Cells were then harvested and lysed, and co-IP was performed using FLAG-tag affinity beads. Immunoprecipitates were run on an immunoblot and stained with the indicated antibodies. (D) HEK293T cells were cotransfected with a FLAG-tagged ORF57 and either an mCherry-empty (mock) or NC-SHFL vector. Cells were then harvested, subjected to immunoblotting, stained with the indicated antibodies, and quantified (E), or total RNA was extracted for RT-qPCR to determine ORF57 mRNA levels (F). ns, not significant. ***, $P < 0.001$. (G) HEK293T cells were transfected with either an mCherry-only (mock) or NC-SHFL vector. Cells were subjected to immunofluorescence assay and stained for the indicated proteins. (H) A zoomed prospective is provided on a cell of interest. Statistics were determined using Student's paired *t* test between control and experimental groups; error bars represent standard errors of the means ($n = 3$ independent biological replicates).

restriction of ORF50 occurs posttranscriptionally and might affect translation rates or protein stability of ORF50 during KSHV infection. It would thus be interesting to investigate the effect of SHFL on lysosome- and proteasome-mediated degradation during KSHV infection, as SHFL has been implicated in these pathways before (22, 25). This restriction of ORF50 early on following lytic reactivation would undoubtedly inhibit many crucial stages of KSHV lytic gene expression and thereby the remainder of lytic viral replication. Previous studies of SHFL have identified at least two SHFL domains that are critical to its capacity to restrict viral infection. Here, we show that the aa 102 to 150 domain, a putative RNA-binding domain, is required bind viral ORF50 mRNA. By virtue of these findings, we conclude that SHFL specifically binds to ORF50 mRNA and that this interaction is critical for its ability to restrict KSHV lytic replication. Whether this domain allows SHFL to exclusively impact ORF50 expression during KSHV infection or, more broadly, the protein stability and/or translation of multiple KSHV early genes remains an important future direction for us.

To better understand the mechanism by which SHFL restricts herpesviral translation, we next mapped the interactome of SHFL during KSHV infection using an IP-MS approach. We found an enrichment of cellular RNA-binding proteins (RBPs) that interact with SHFL during both KSHV latency and lytic reactivation. These include a vital host translation factor and previously identified SHFL interactor, PABPC1. We also identified several other RBPs that are known constituents of cytoplasmic RNP granules, including both P-bodies and stress granules. Both granule types have gained increasing attention over the past decade as critical biophysical sites of RNA regulation that have recently been attributed both pro- and antiviral functions (58–61). Here, we show for the first time that transient expression of SHFL alone triggers the disassembly of P-bodies and simultaneously the induction SG-like densities in virus-free cells. Interestingly, in KSHV-positive cells, we observed a similar reduction in P-bodies during both viral latency and lytic replication but have yet to determine whether an impact can be observed on SG formation. It is important to note that previous studies have already demonstrated that P-bodies are lost during KSHV lytic replication through a variety of mechanisms and so we are unable to determine with certainty whether the loss of P-bodies in lytic cells transfected with SHFL is due solely to the functions of SHFL (62–65). Whether the loss of SHFL also leads to an increased number of P-bodies during latency and lytic replication remains to be assessed. If SHFL further enhances KSHV P-body restriction, it could suggest that SHFL restriction of P-bodies contributes to an antiviral state and calls into question the strictly antiviral nature of this RNA granule type during KSHV infection. The SG-like densities we have observed by SHFL suggests that the functions of SHFL likely impact global cellular translation more broadly than initially anticipated, perhaps restricting the translation of several host genes, which could, in turn, influence P-body assembly and/or scaffolding factor localization. These dynamics between SHFL, a known ISG, and RNA granules raises several questions regarding the antiviral capacity of P-bodies during KSHV infection, such as the following: (i) do P-bodies also have an unforeseen proviral role given their disassembly by SHFL, (ii) are transcripts targeted by SHFL localized to SHFL-induced SGs for translational arrest, and (iii) what part of the SHFL mechanism is responsible for its influence over RNP granules? Moving forward, we are interested in exploring the breadth of both viral and cellular transcripts that are targeted by SHFL in KSHV-infected cells.

The relationship between KSHV and RNA granules is multilayered. While P-bodies are constitutively formed in cells, SGs only form in response to cellular stressors such as oxidative stress and, relevantly, viral infection. P-body dynamics during KSHV latency remains an active area of research to better understand what viral and host factors regulate their stability (52, 62, 63). However, it has been clearly established that during lytic replication, KSHV actively disassembles P-bodies and restricts the formation of SGs. This restriction of RNP granules during lytic replication is directly facilitated by the viral protein KSHV ORF57 (52, 64). ORF57 is a master regulator of KSHV viral RNA fate with roles including viral mRNA splicing, nuclear mRNA export, and even facilitation of viral mRNA translation in the cytoplasm (42, 66, 67). Therefore, we were keenly

interested in understanding the relationship between SHFL and ORF57. In this study, we found that SHFL does in fact interact with ORF57 in an RNA-dependent manner. To better assess the specificity of this interaction, we also tested whether ORF57 could still interact with SHFLΔ102-150 and found that the loss of this domain resulted in a breaking of the SHFL-ORF57 interaction. These results highlight the importance of RNA as an intermediary between these two versatile RNA-binding proteins. Therefore, we next probed the same immunoprecipitates of cells expressing both SHFL and ORF57 and confirmed strong interactions between SHFL, PABPC1, and DDX3X and weak interactions with FUS and KPNA2, all hits found within our IP-MS screen. Defining the SHFL-ORF57 complex to better the understand the impact of SHFL on viral gene expression will bring important insights into the regulation of lytic infection. Interestingly, we also observed a downregulation of ORF57 expression when ORF57 was coexpressed alongside SHFL. Notably, there was no impact of SHFL on ORF57 mRNA levels, which in combination with our observations of ORF50 further suggests that SHFL also targets ORF57 expression at the protein level. Given its ability to influence RNP granules, we next investigated whether ORF57 could restrict the formation of SHFL-induced SG-like densities. Surprisingly, we found that SGs were still restricted by ORF57 despite its distinct downregulation by SHFL. In their place, we observed distinct accumulations of ORF57, SHFL, and the SG marker TIA-1 in the cytoplasm. These SHFL-ORF57 densities could reflect sites of translational arrest by SHFL on ORF57 specifically. However, they may also suggest that there could be a distinct difference in the RNP composition of SHFL-induced SGs that could be tailored toward a response to viral genes versus host genes. Further exploration is required to determine if SHFL also restricts the translation of ORF57. Or, as suggested by recent SHFL studies in Zika virus (ZIKV), porcine epidemic diarrheal virus (PEDV), and JEV, SHFL could coordinate with lysosomal or ubiquitinoylation pathways to degrade ORF57 (22, 25, 26).

In conclusion, our findings lay the foundation for a complex relationship between SHFL, a potent antiviral factor, and the DNA virus KSHV. Following the escape of SHFL mRNA from SOX cleavage, SHFL protein levels climb over the course of KSHV lytic replication. SHFL expression restricts both KSHV early and delayed early genes in a manner that cascades out to late gene expression, an effect whose ramifications are evident across every step of KSHV lytic replication. Here, we show for the first time that overexpression of SHFL influences the formation of cytoplasmic RNA granules, namely, stress granules and processing bodies. Thus, SHFL may restrict herpesviral gene expression at a stage between viral protein stability and viral gene translation. This impact on RNP granules also suggests that SHFL's mechanism of action has much broader repercussions on global cellular translation. And therein, SHFL could restrict the translation of host genes that play proviral roles in the earliest stages of lytic replication. Among the interactions of SHFL, ORF57 also represents a cornerstone of lytic gene expression initiation and countless roles in the stability of viral mRNAs during infection. Therefore, SHFL could also target ORF57 as well as ORF50 and, through this two-pronged assault, cripple KSHV replication. Thus, we may begin to piece together a model in which, following its escape from SOX cleavage, the C19ORF66 mRNA encodes the potent antiviral protein SHFL. As we have shown before, SHFL endogenous expression rises over the course of lytic reactivation, and we hypothesized that past a certain level, SHFL restricts lytic gene expression by either directly or indirectly targeting the expression of the master latent-to-lytic switch protein KSHV ORF50 (RTA). From there, a cascade of restriction is triggered, with the restriction of ORF50 leading to the repression of virtually all lytic viral genes. By studying the impact of SHFL on KSHV lytic reactivation, we continue to unravel unexpected relationships between the regulation cellular RNA fate and the virus-host arms race for control of global gene expression during herpesviral infection.

MATERIALS AND METHODS

Cells and transfections. HEK293T cells (ATCC) were grown in Dulbecco's modified Eagle's medium (DMEM; Invitrogen) supplemented with 10% fetal bovine serum (FBS). The KSHV-infected renal carcinoma human cell line iSLK.BAC16 (iSLK.WT) (kind gift from B. Glaunsinger) bearing doxycycline-inducible RTA

was grown in DMEM supplemented with 10% FBS (68, 69). KSHV lytic reactivation was induced by the addition of 1 μg/mL of doxycycline (BD Biosciences) and 1 mM sodium butyrate for 48 h as reported above. For DNA transfections, cells were plated and transfected after 24 h when 70% confluent using PolyJet (SignaGen). For small interfering RNA (siRNA) transfections, cells were reverse transfected in 6-well plates by INTERFERin (Polyplus) with 10 μM siRNAs. siRNAs were obtained from IDT as Dicer-substrate siRNA (DsiRNA; siRNA C19ORF66, hs.Ri.C19orf66.13.1).

Plasmids. The C19ORF66 coding region was obtained as a gBlock from IDT and cloned into a pcDNA4 Nter-3×FLAG vector (FLAG-SHFL). The SHFL coding region was then cloned into a pmCherry-C1 vector (kind gift from Jeffrey Kane) to construct the N-terminal mCherry-C19ORF66 vector (NC-SHFL). A FLAG-empty vector (pcDNA4 Nter 3×FLAG) or mCherry only (pmCherry-C1) was used as a control where indicated. KSHV lytic gene coding sequences (ORF50, ORF57, ORF59, and ORF52) were derived from a library of strep-tagged KSHV ORFs (70) and cloned into recipient vectors to construct ORF57-6×HIS and FLAG-ORF57.

RT-qPCR. Total RNA was harvested using TRIzol according to the manufacturer's protocol. cDNAs were synthesized from 1 μg of total RNA using avian myeloblastosis virus (AMV) reverse transcriptase (Promega) and used directly for quantitative PCR (qPCR) analysis with the SYBR green qPCR kit (Bio-Rad). Signals obtained by qPCR were normalized to those for 18S RNA unless otherwise noted. Primers used in the study are listed in Table S3.

Immunoblotting. Cell lysates were prepared in lysis buffer (NaCl, 150 mM; Tris, 50 mM; NP-40, 0.5%; dithiothreitol [DTT], 1 mM; and protease inhibitor tablets) and quantified by Bradford assay. Equivalent amounts of each sample were resolved by SDS-PAGE and immunoblotted with each respective antibody at 1:1,000 in TBST (Tris-buffered saline, 0.1% Tween 20). Antibodies used for human and KSHV targets are listed in Table S4. Primary antibody incubations were followed by incubations with horseradish peroxidase (HRP)-conjugated goat anti-mouse or goat anti-rabbit secondary antibodies (1:5,000; Southern Biotechnology).

Immunoprecipitation. Cells were lysed in low-salt lysis buffer (150 mM NaCl, 0.5% NP-40, 50 mM Tris [pH 8], 1 mM DTT, and protease inhibitor cocktail), and protein concentrations were determined by Bradford assay. At least 400 μg of total protein was incubated overnight with the designated antibody and then with protein G-coupled magnetic beads (Life Technologies) for 1 h. For FLAG construct pulldowns, total protein lysates were instead incubated overnight with anti-FLAG M2 magnetic beads (Sigma) or G-coupled magnetic beads. Beads were then washed extensively with lysis buffer. Where indicated, samples were treated with both RNase A and T1 for 15 min at room temperature prior to immunoprecipitation. Lastly, samples were resuspended in 4× Laemmli loading dye before resolution by SDS-PAGE.

Mass spectrometry. Briefly, iSLK.WT cells were seeded into 10-cm plates and reactivated at the same time. At 72 h postreactivation, cells were harvested and lysed, and immunoprecipitation for SHFL was performed overnight at 4°C. Samples were extensively washed and were trypsin digested overnight. Samples were then cleaned up using a C_{18} column and mass spectral data were obtained from the University of Massachusetts Mass Spectrometry Center using an Orbitrap Fusion mass spectrometer. Raw data were filtered based on the number of peptides for each hit and Gene Ontology (GO) enrichment analysis was performed on the human interacting proteins of SHFL using the DAVID bioinformatic database. Top enriched clusters are identified on the network.

RIP. Following transfections, cells were cross-linked in 1% formaldehyde for 10 min, quenched in 125 mM glycine, and washed in phosphate-buffered saline (PBS). Cells were then lysed in low-salt lysis buffer (NaCl [150 mM], NP-40 [0.5%], Tris [pH 8; 50 mM], DTT [1 mM], $MgCl_2$ [3 mM] containing protease inhibitor cocktail and RNase inhibitor) and sonicated. After removal of cell debris, anti-FLAG M2 magnetic beads or magnetic G-coupled beads were added overnight at 4°C as indicated. The following day, beads were washed three times with lysis buffer and twice with high-salt lysis buffer (low-salt lysis buffer except containing 400 mM NaCl). Samples were then separated into two fractions. Beads containing the fraction used for immunoblotting were resuspended in 30 μL of lysis buffer. Beads containing the fraction used for RNA extraction were resuspended in proteinase K (PK) buffer (NaCl [100 mM], Tris [pH 7.4; 10 mM], EDTA [1 mM], SDS [0.5%]) containing 1 μL of PK. Samples were incubated overnight at 65°C to reverse cross-linking. Samples to be analyzed by immunoblotting were then supplemented with 10 μL of 4× loading buffer before resolution by SDS-PAGE. RNA samples were resuspended in TRIzol, and total RNA was extracted for qPCR as described above.

4sU labeling. Following transfection of either FLAG-empty or FLAG-SHFL and 48 h postreactivation, iSLK.WT cells were pulse-labeled with DMEM containing 500 μM 4sU (Sigma) for 10 min, followed by a PBS wash and immediate isolation of total RNA with TRIzol. 4sU isolation was performed as previously described (11). 4sU isolated RNA was analyzed by RT-qPCR for the indicated genes.

RNA half-life. iSLK.WT cells were plated and transfected with either an mCherry-only (mock) or NC-SHFL vector. Twenty-four hours later, KSHV was reactivated as described above for roughly 40 h. Six hours prior to the 48-h time point, transfected cells were treated with 5 μg/mL of actinomycin D to inhibit cellular transcription and cells were collected at the indicated time points from 0 to 8 h. Total RNA was extracted from all samples, subjected to qPCR analysis using primers targeting KSHV ORF50, and normalized to the level of glyceraldehyde-3-phosphate dehydrogenase (GAPDH) mRNA.

Immunofluorescence. HEK293T or iSLK.WT cells were grown on coverslips and fixed in 4% formaldehyde for 20 min at room temperature. Cells were then permeabilized in 1% Triton X-100 and 0.1% sodium citrate in PBS for 10 min, saturated in bovine serum albumin (BSA) for 30 min, and incubated with the designated antibodies at various dilutions (Table S2). After 1 h, coverslips were washed in PBS and incubated with Alexa Fluor 680, 594, or 488 secondary antibody at 1:1,500 (Invitrogen). Coverslips were washed again in PBS and mounted in 4′,6-diamidino-2-phenylindole (DAPI)-containing Vectashield

mounting medium (Vector Labs) to stain cell nuclei before visualization by confocal microscopy on a Nikon A1 resonant scanning confocal microscope (A1R-SIMe). The microscopy data were gathered in the Light Microscopy Facility and Nikon Center of Excellence at the Institute for Applied Life Sciences, UMass Amherst, with support from the Massachusetts Life Sciences Center.

RNA granule quantification. Processing bodies and stress granules were quantified using an unbiased image analysis pipeline generated in the freeware CellProfiler (https://cellprofiler.org/) (63, 69, 71). First, detection of nuclei in the DAPI channel image was performed by applying a binary threshold and executing primary object detection between 50 and 250 pixels. From each identified nuclear object, the "Propagation" function was performed on the respective 594 channel (denoting mock [mCherry] or NC-SHFL) image to define transfected cell borders. The identified cell borders were masked with the identified nuclei to define a cytoplasm mask. The cytoplasm mask was then applied to the processing body/stress granule punctum channel images (stains with DDX6 and EDC4 for processing bodies) to ensure that only cytoplasmic puncta were quantified. Background staining was reduced in the cytoplasmic punctum channel using the "Enhance Speckles" function. Using "global thresholding with robust background adjustments," puncta within a defined size and intensity range were quantified. Size and intensity thresholds were unchanged between experiments with identical staining parameters. Intensity measurements of puncta were quantified. Quantification data were exported and used for data analysis.

Statistical analysis. All results are expressed as means ± standard errors of the means (SEMs) of experiments independently repeated at least three times. Unpaired Student's *t* test was used to evaluate the statistical difference between samples.

SUPPLEMENTAL MATERIAL

Supplemental material is available online only.

SUPPLEMENTAL FILE 1, PDF file, 1 MB.

ACKNOWLEDGMENTS

We thank all members of the Muller lab for helpful discussions and suggestions. Special thanks go to Britt Glaunsinger for both our iSLK cell lines and KSHV antibodies. We are also particularly grateful to Jennifer Corcoran and Beth Castle for our conversations and their suggestions with RNA granule detection and quantification. We also thank James Chambers at the UMASS IALS Light Microscope Facility and Stephen Eyles at the UMASS IALS Mass Spectrometry Facility for their help with protocol development and data acquisition.

This research was supported by the UMass Microbiology Startup fund and NIH grant R35GM138043 to M.M.

REFERENCES

1. Iftode N, Rădulescu MA, Aramă ȘS, Aramă V. 2020. Update on Kaposi sarcoma-associated herpesvirus (KSHV or HHV8)—review. Rom J Intern Med 58:199–208. https://doi.org/10.2478/rjim-2020-0017.
2. Sung H, Ferlay J, Siegel RL, Laversanne M, Soerjomataram I, Jemal A, Bray F. 2021. Global cancer statistics 2020: GLOBOCAN estimates of incidence and mortality worldwide for 36 cancers in 185 countries. CA Cancer J Clin 71:209–249. https://doi.org/10.3322/caac.21660.
3. Broussard G, Damania B. 2020. Regulation of KSHV latency and lytic reactivation. Viruses 12:1034. https://doi.org/10.3390/v12091034.
4. Aneja KK, Yuan Y. 2017. Reactivation and lytic replication of Kaposi's sarcoma-associated herpesvirus: an update. Front Microbiol 8:613. https://doi.org/10.3389/fmicb.2017.00613.
5. Manners O, Murphy JC, Coleman A, Hughes DJ, Whitehouse A. 2018. Contribution of the KSHV and EBV lytic cycles to tumourigenesis. Curr Opin Virol 32:60–70. https://doi.org/10.1016/j.coviro.2018.08.014.
6. Yan L, Majerciak V, Zheng Z-M, Lan K. 2019. Towards better understanding of KSHV life cycle: from transcription and posttranscriptional regulations to pathogenesis. Virol Sin 34:135–161. https://doi.org/10.1007/s12250-019-00114-3.
7. Covarrubias S, Richner JM, Clyde K, Lee YJ, Glaunsinger BA. 2009. Host shutoff is a conserved phenotype of gammaherpesvirus infection and is orchestrated exclusively from the cytoplasm. J Virol 83:9554–9566. https://doi.org/10.1128/JVI.01051-09.
8. Covarrubias S, Gaglia MM, Kumar GR, Wong W, Jackson AO, Glaunsinger BA. 2011. Coordinated destruction of cellular messages in translation complexes by the gammaherpesvirus host shutoff factor and the mammalian exonuclease Xrn1. PLoS Pathog 7:e1002339. https://doi.org/10.1371/journal.ppat.1002339.
9. Glaunsinger B, Ganem D. 2004. Lytic KSHV infection inhibits host gene expression by accelerating global mRNA turnover. Mol Cell 13:713–723. https://doi.org/10.1016/S1097-2765(04)00091-7.
10. Richner JM, Clyde K, Pezda AC, Cheng BYH, Wang T, Kumar GR, Covarrubias S, Coscoy L, Glaunsinger B. 2011. Global mRNA degradation during lytic gammaherpesvirus infection contributes to establishment of viral latency. PLoS Pathog 7:e1002150. https://doi.org/10.1371/journal.ppat.1002150.
11. Abernathy E, Gilbertson S, Alla R, Glaunsinger B. 2015. Viral nucleases induce an mRNA degradation-transcription feedback loop in mammalian cells. Cell Host Microbe 18:243–253. https://doi.org/10.1016/j.chom.2015.06.019.
12. Gilbertson S, Federspiel JD, Hartenian E, Cristea IM, Glaunsinger B. 2018. Changes in mRNA abundance drive shuttling of RNA binding proteins, linking cytoplasmic RNA degradation to transcription. Elife 7:e37663. https://doi.org/10.7554/eLife.37663.
13. Clyde K, Glaunsinger BA. 2011. Deep sequencing reveals direct targets of gammaherpesvirus-induced mRNA decay and suggests that multiple mechanisms govern cellular transcript escape. PLoS One 6:e19655. https://doi.org/10.1371/journal.pone.0019655.
14. Muller M, Hutin S, Marigold O, Li KH, Burlingame A, Glaunsinger BA. 2015. A ribonucleoprotein complex protects the interleukin-6 mRNA from degradation by distinct herpesviral endonucleases. PLoS Pathog 11:e1004899. https://doi.org/10.1371/journal.ppat.1004899.
15. Glaunsinger B, Ganem D. 2004. Highly selective escape from KSHV-mediated host mRNA shutoff and its implications for viral pathogenesis. J Exp Med 200:391–398. https://doi.org/10.1084/jem.20031881.
16. Hutin S, Lee Y, Glaunsinger BA. 2013. An RNA element in human interleukin 6 confers escape from degradation by the gammaherpesvirus SOX protein. J Virol 87:4672–4682. https://doi.org/10.1128/JVI.00159-13.
17. Muller M, Glaunsinger BA. 2017. Nuclease escape elements protect messenger RNA against cleavage by multiple viral endonucleases. PLoS Pathog 13:e1006593. https://doi.org/10.1371/journal.ppat.1006593.

18. Rodriguez W, Srivastav K, Muller M. 2019. C19ORF66 broadly escapes virus-induced endonuclease cleavage and restricts Kaposi's sarcoma-associated herpesvirus. J Virol 93:e00373-19. https://doi.org/10.1128/JVI.00373-19.
19. Suzuki Y, Chin W-X, Han Q, Ichiyama K, Lee CH, Eyo ZW, Ebina H, Takahashi H, Takahashi C, Tan BH, Hishiki T, Ohba K, Matsuyama T, Koyanagi Y, Tan Y-J, Sawasaki T, Chu JJH, Vasudevan SG, Sano K, Yamamoto N. 2016. Characterization of RyDEN (C19orf66) as an interferon-stimulated cellular inhibitor against dengue virus replication. PLoS Pathog 12:e1005357. https://doi.org/10.1371/journal.ppat.1005357.
20. Balinsky CA, Schmeisser H, Wells AI, Ganesan S, Jin T, Singh K, Zoon KC. 2017. IRAV (FLJ11286), an interferon-stimulated gene with antiviral activity against dengue virus, interacts with MOV10. J Virol 91:e01606-16. https://doi.org/10.1128/JVI.01606-16.
21. Wang X, Xuan Y, Han Y, Ding X, Ye K, Yang F, Gao P, Goff SP, Gao G. 2019. Regulation of HIV-1 Gag-Pol expression by shiftless, an inhibitor of programmed -1 ribosomal frameshifting. Cell 176:625–635.e14. https://doi.org/10.1016/j.cell.2018.12.030.
22. Wu Y, Yang X, Yao Z, Dong X, Zhang D, Hu Y, Zhang S, Lin J, Chen J, An S, Ye H, Zhang S, Qiu Z, He Z, Huang M, Wei G, Zhu X. 2020. C19orf66 interrupts Zika virus replication by inducing lysosomal degradation of viral NS3. PLoS Negl Trop Dis 14:e0008083. https://doi.org/10.1371/journal.pntd.0008083.
23. Kinast V, Plociennikowska A, Bracht T, Todt D, Brown RJP, Boldanova T, Zhang Y, Brüggemann Y, Friesland M, Engelmann M, Vieyres G, Broering R, Vondran FWR, Heim MH, Sitek B, Bartenschlager R, Pietschmann T, Steinmann E, Anggakusuma. 2020. C19orf66 is an interferon-induced inhibitor of HCV replication that restricts formation of the viral replication organelle. J Hepatol 73:549–558. https://doi.org/10.1016/j.jhep.2020.03.047.
24. Sun Y, Abriola L, Niederer RO, Pedersen SF, Alfajaro MM, Silva Monteiro V, Wilen CB, Ho Y-C, Gilbert WV, Surovtseva YV, Lindenbach BD, Guo JU. 2021. Restriction of SARS-CoV-2 replication by targeting programmed −1 ribosomal frameshifting. Proc Natl Acad Sci U S A 118:e2023051118. https://doi.org/10.1073/pnas.2023051118.
25. Wang H, Kong N, Jiao Y, Dong S, Sun D, Chen X, Zheng H, Tong W, Yu H, Yu L, Zhang W, Tong G, Shan T. 2021. EGR1 suppresses porcine epidemic diarrhea virus replication by regulating IRAV to degrade viral nucleocapsid protein. J Virol 95:e00645-21. https://doi.org/10.1128/JVI.00645-21.
26. Yu D, Zhao Y, Pan J, Yang X, Liang Z, Xie S, Cao R. 2021. C19orf66 inhibits Japanese encephalitis virus replication by targeting −1 PRF and the NS3 protein. Virol Sin 36:1443–1455. https://doi.org/10.1007/s12250-021-00423-6.
27. Hanners NW, Mar KB, Boys IN, Eitson JL, De La Cruz-Rivera PC, Richardson RB, Fan W, Wight-Carter M, Schoggins JW. 2021. Shiftless inhibits flavivirus replication in vitro and is neuroprotective in a mouse model of Zika virus pathogenesis. Proc Natl Acad Sci U S A 118:e2111266118. https://doi.org/10.1073/pnas.2111266118.
28. Napthine S, Hill CH, Nugent HC, Brierley I. 2021. Modulation of viral programmed ribosomal frameshifting and stop codon readthrough by the host restriction factor shiftless. Viruses 13:1230. https://doi.org/10.3390/v13071230.
29. Rodriguez W, Muller M. 2022. Shiftless, a critical piece of the innate immune response to viral infection. Viruses 14:1338. https://doi.org/10.3390/v14061338.
30. Lukac DM, Kirshner JR, Ganem D. 1999. Transcriptional activation by the product of open reading frame 50 of Kaposi's sarcoma-associated herpesvirus is required for lytic viral reactivation in B cells. J Virol 73:9348–9361. https://doi.org/10.1128/JVI.73.11.9348-9361.1999.
31. Guito J, Lukac DM. 2012. KSHV Rta promoter specification and viral reactivation. Front Microbiol 3:30. https://doi.org/10.3389/fmicb.2012.00030.
32. Kaul R, Purushothaman P, Uppal T, Verma SC. 2019. KSHV lytic proteins K-RTA and K8 bind to cellular and viral chromatin to modulate gene expression. PLoS One 14:e0215394. https://doi.org/10.1371/journal.pone.0215394.
33. He M. 2019. Molecular biology of KSHV in relation to HIV/AIDS-associated oncogenesis, p 23–62. *In* Meyers C (ed), HIV/AIDS-associated viral oncogenesis. Springer, Cham, Switzerland.
34. Myoung J, Ganem D. 2011. Infection of lymphoblastoid cell lines by Kaposi's sarcoma-associated herpesvirus: critical role of cell-associated virus. J Virol 85:9767–9777. https://doi.org/10.1128/JVI.05136-11.
35. Hesser CR, Karijolich J, Dominissini D, He C, Glaunsinger BA. 2018. N 6-methyladenosine modification and the YTHDF2 reader protein play cell type specific roles in lytic viral gene expression during Kaposi's sarcoma-associated herpesvirus infection. PLoS Pathog 14:e1006995. https://doi.org/10.1371/journal.ppat.1006995.
36. Gradoville L, Gerlach J, Grogan E, Shedd D, Nikiforow S, Metroka C, Miller G. 2000. Kaposi's sarcoma-associated herpesvirus open reading frame 50/Rta protein activates the entire viral lytic cycle in the HH-B2 primary effusion lymphoma cell line. J Virol 74:6207–6212. https://doi.org/10.1128/JVI.74.13.6207-6212.2000.
37. Fujimura K, Suzuki T, Yasuda Y, Murata M, Katahira J, Yoneda Y. 2010. Identification of importin α1 as a novel constituent of RNA stress granules. Biochim Biophys Acta 1803:865–871. https://doi.org/10.1016/j.bbamcr.2010.03.020.
38. Valentin-Vega YA, Wang Y-D, Parker M, Patmore DM, Kanagaraj A, Moore J, Rusch M, Finkelstein D, Ellison DW, Gilbertson RJ, Zhang J, Kim HJ, Taylor JP. 2016. Cancer-associated DDX3X mutations drive stress granule assembly and impair global translation. Sci Rep 6:25996. https://doi.org/10.1038/srep25996.
39. Yasuda K, Zhang H, Loiselle D, Haystead T, Macara IG, Mili S. 2013. The RNA-binding protein Fus directs translation of localized mRNAs in APC-RNP granules. J Cell Biol 203:737–746. https://doi.org/10.1083/jcb.201306058.
40. Fukuda T, Naiki T, Saito M, Irie K. 2009. hnRNP K interacts with RNA binding motif protein 42 and functions in the maintenance of cellular ATP level during stress conditions. Genes Cells 14:113–128. https://doi.org/10.1111/j.1365-2443.2008.01256.x.
41. Hiura K, Strahan R, Uppal T, Prince B, Rossetto CC, Verma SC. 2020. KSHV ORF59 and pan RNA recruit histone demethylases to the viral chromatin during lytic reactivation. Viruses 12:420. https://doi.org/10.3390/v12040420.
42. Majerciak V, Zheng ZM. 2015. KSHV ORF57, a protein of many faces. Viruses 7:604–633. https://doi.org/10.3390/v7020604.
43. Li W, Avey D, Fu B, Wu JJ, Ma S, Liu X, Zhu F. 2016. Kaposi's sarcoma-associated herpesvirus inhibitor of cGAS (KicGAS), encoded by ORF52, is an abundant tegument protein and is required for production of infectious progeny viruses. J Virol 90:5329–5342. https://doi.org/10.1128/JVI.02675-15.
44. Corbet GA, Parker R. 2019. RNP granule formation: lessons from P-bodies and stress granules. Cold Spring Harbor Symp Quant Biol 84:203–215. https://doi.org/10.1101/sqb.2019.84.040329.
45. Tauber D, Tauber G, Parker R. 2020. Mechanisms and regulation of RNA condensation in RNP granule formation. Trends Biochem Sci 45:764–778. https://doi.org/10.1016/j.tibs.2020.05.002.
46. Riggs CL, Kedersha N, Ivanov P, Anderson P. 2020. Mammalian stress granules and P bodies at a glance. J Cell Sci 133:jcs242487. https://doi.org/10.1242/jcs.242487.
47. Tian S, Curnutte HA, Trcek T. 2020. RNA granules: a view from the RNA perspective. Molecules 25:3130. https://doi.org/10.3390/molecules25143130.
48. Anderson P, Kedersha N, Ivanov P. 2015. Stress granules, P-bodies and cancer. Biochim Biophys Acta 1849:861–870. https://doi.org/10.1016/j.bbagrm.2014.11.009.
49. Fan AC, Leung AKL. 2016. RNA granules and diseases: a case study of stress granules in ALS and FTLD. Adv Exp Med Biol 907:263–296. https://doi.org/10.1007/978-3-319-29073-7_11.
50. Kedersha N, Anderson P. 2007. Mammalian stress granules and processing bodies. Methods Enzymol 431:61–81. https://doi.org/10.1016/S0076-6879(07)31005-7.
51. Guzikowski AR, Chen YS, Zid BM. 2019. Stress-induced mRNP granules: form and function of processing bodies and stress granules. Wiley Interdiscip Rev RNA 10:e1524.
52. Sharma NR, Majerciak V, Kruhlak MJ, Yu L, Kang JG, Yang A, Gu S, Fritzler MJ, Zheng Z-M. 2019. KSHV RNA-binding protein ORF57 inhibits P-body formation to promote viral multiplication by interaction with Ago2 and GW182. Nucleic Acids Res 47:9368–9385. https://doi.org/10.1093/nar/gkz683.
53. Piecyk M, Wax S, Beck AR, Kedersha N, Gupta M, Maritim B, Chen S, Gueydan C, Kruys V, Streuli M, Anderson P. 2000. TIA-1 is a translational silencer that selectively regulates the expression of TNF-α. EMBO J 19:4154–4163. https://doi.org/10.1093/emboj/19.15.4154.
54. Díaz-Muñoz MD, Kiselev VY, Le Novère N, Curk T, Ule J, Turner M. 2017. Tia1 dependent regulation of mRNA subcellular location and translation controls p53 expression in B cells. Nat Commun 8:530. https://doi.org/10.1038/s41467-017-00454-2.
55. Penn WD, Harrington HR, Schlebach JP, Mukhopadhyay S. 2020. Regulators of viral frameshifting: more than RNA influences translation events. Annu Rev Virol 7:219–238. https://doi.org/10.1146/annurev-virology-012120-101548.
56. Clark MB, Janicke M, Gottesbuhren U, Kleffmann T, Legge M, Poole ES, Tate WP. 2007. Mammalian gene PEG10 expresses two reading frames by high efficiency −1 frameshifting in embryonic-associated tissues. J Biol Chem 282:37359–37369. https://doi.org/10.1074/jbc.M705676200.

57. Belew AT, Meskauskas A, Musalgaonkar S, Advani VM, Sulima SO, Kasprzak WK, Shapiro BA, Dinman JD. 2014. Ribosomal frameshifting in the CCR5 mRNA is regulated by miRNAs and the NMD pathway. Nature 512:265–269. https://doi.org/10.1038/nature13429.
58. Kanakamani S, Suresh PS, Venkatesh T. 2021. Regulation of processing bodies: from viruses to cancer epigenetic machinery. Cell Biol Int 45:708–719. https://doi.org/10.1002/cbin.11527.
59. Scoca V, Di Nunzio F. 2021. Membraneless organelles restructured and built by pandemic viruses: HIV-1 and SARS-CoV-2. J Mol Cell Biol 13:259–268. https://doi.org/10.1093/jmcb/mjab020.
60. Zhang Q, Sharma NR, Zheng ZM, Chen M. 2019. Viral regulation of RNA granules in infected cells. Virol Sin 34:175–191. https://doi.org/10.1007/s12250-019-00122-3.
61. Lloyd RE. 2013. Regulation of stress granules and P-bodies during RNA virus infection. Wiley Interdiscip Rev RNA 4:317–331. https://doi.org/10.1002/wrna.1162.
62. Corcoran JA, McCormick C. 2015. Viral activation of stress-regulated Rho-GTPase signaling pathway disrupts sites of mRNA degradation to influence cellular gene expression. Small GTPases 6:178–185. https://doi.org/10.1080/21541248.2015.1093068.
63. Castle EL, Robinson CA, Douglas P, Rinker KD, Corcoran JA. 2021. Viral manipulation of a mechanoresponsive signaling axis disassembles processing bodies. Mol Cell Biol 41:e00399-21. https://doi.org/10.1128/MCB.00399-21.
64. Sharma NR, Majerciak V, Kruhlak MJ, Zheng ZM. 2017. KSHV inhibits stress granule formation by viral ORF57 blocking PKR activation. PLoS Pathog 13:e1006677. https://doi.org/10.1371/journal.ppat.1006677.
65. Sharma NR, Zheng ZM. 2021. RNA granules in antiviral innate immunity: a Kaposi's sarcoma-associated herpesvirus journey. Front Microbiol 12:794431.
66. Ruiz JC, Devlin AM, Kim J, Conrad NK. 2020. Kaposi's sarcoma-associated herpesvirus fine-tunes the temporal expression of late genes by manipulating a host RNA quality control pathway. J Virol 94:e00287-20. https://doi.org/10.1128/JVI.00287-20.
67. Ruiz JC, Hunter OV, Conrad NK. 2019. Kaposi's sarcoma-associated herpesvirus ORF57 protein protects viral transcripts from specific nuclear RNA decay pathways by preventing hMTR4 recruitment. PLoS Pathog 15:e1007596. https://doi.org/10.1371/journal.ppat.1007596.
68. Brulois KF, Chang H, Lee AS-Y, Ensser A, Wong L-Y, Toth Z, Lee SH, Lee H-R, Myoung J, Ganem D, Oh T-K, Kim JF, Gao S-J, Jung JU. 2012. Construction and manipulation of a new Kaposi's sarcoma-associated herpesvirus bacterial artificial chromosome clone. J Virol 86:9708–9720.
69. Robinson C-A, Singh GK, Castle EL, Boudreau BQ, Corcoran JA. 2021. The NDP52/CALCOCO2 selective autophagy receptor controls processing body disassembly. bioRxiv. https://doi.org/10.1101/2021.02.07.430164.
70. Davis ZH, Verschueren E, Jang GM, Kleffman K, Johnson JR, Park J, Dollen JV, Maher CM, Johnson T, Newton W, Jäger S, Shales M, Horner J, Hernandez RD, Krogan NJ, Glaunsinger BA. 2015. Global mapping of herpesvirus-host protein complexes reveals a transcription strategy for late genes. Mol Cell 57:349–360. https://doi.org/10.1016/j.molcel.2014.11.026.
71. Kleer M, Mulloy RP, Robinson C-A, Evseev D, Bui-Marinos MP, Castle EL, Banerjee A, Mubareka S, Mossman K, Corcoran JA. 2020. Human coronaviruses disassemble processing bodies. bioRxiv. https://doi.org/10.1101/2020.11.08.372995.